Journal of Alloys and Compounds 827 (2020) 154305

Contents lists available at ScienceDirect

Journal of Alloys and Compounds

journal homepage: http://www.elsevier.com/locate/jalcom

Enhanced mechanical properties of high-temperature-resistant Al–Cu cast alloy by microalloying with Mg

Jovid Rakhmonov [a], Kun Liu [a, *], Lei Pan [b], Francis Breton [b], X.-Grant Chen [a]

[a] Department of Applied Sciences, University of Quebec in Chicoutimi, Saguenay, Quebec, G7H 2B1, Canada
[b] Arvida Research and Development Centre, Rio Tinto Aluminum, Saguenay, Quebec, G7S 4K8, Canada

ARTICLE INFO

Article history:
Received 18 November 2019
Accepted 11 February 2020
Available online 13 February 2020

Keywords:
Al–Cu alloys
Mg microalloying
Microstructure
Mechanical properties
High-temperature strength
Precipitation

ABSTRACT

The effects of microalloying with Mg (0–0.23 wt%) on the microstructural evolution and mechanical properties of Al–Cu 224 cast alloys at ambient and elevated temperatures are investigated using transmission electron microscopy, differential scanning calorimetry, and tensile/compression testing. The results show that microalloying with Mg significantly enhances the precipitation of the θ′ phase during aging, producing fine, dense, and uniformly distributed θ′ precipitates. These precipitates are much more effective for alloy strengthening than are the θ″ precipitates in the alloy without Mg. During stabilization at 300 °C for 100 h, the dominant process becomes coarsening of the θ′ phase. The Mg-containing alloys have much finer and denser θ′ precipitates and thus considerably higher yield strengths at elevated temperature as compared to those of the alloy without Mg. The improvement is more pronounced at low Mg contents (0.09%–0.13%) than at high contents. The yield strength at 300 °C of the 0.13% Mg alloy is as high as 140 MPa, which is far superior to that of most cast aluminum alloys. Moreover, the enhanced yield strength of this alloy is well preserved during prolonged exposure at 300 °C for 1000 h, indicating that it is a promising lightweight material for high-temperature applications.

1. Introduction

Weight reduction has become a prominent approach to improving fuel efficiency and reducing greenhouse gas emissions in the automotive industry; consequently, Al-based alloys are finding new applications, some of which require exposure to high stress and temperature during service [1]. Engine blocks and cylinder heads, for instance, must withstand high operating temperatures and stress [1,2]. Various cast alloy systems, such as Al–Cu, Al–Si–Cu–Mg, and Al–Si–Mg, have been adopted for engine applications. The most commonly used systems are Al–Si–Mg (356 type) and Al–Si–Cu–Mg (319 type) cast alloys, as they offer excellent castability and relatively high ambient-temperature mechanical properties. The improved mechanical properties are primarily provided by metastable, nanoscale strengthening precipitates such as β″ (a Mg_2Si precursor) in 356 alloys and θ′ (an Al_2Cu precursor) in 319 alloys. However, these precipitates exhibit limited thermal stability at temperatures above 200 °C, causing a sharp decrease in the mechanical properties [3]. The expected enhancement of engine power in the near future is anticipated to raise the operating temperature of engines to 300–350 °C [4,5]. Thus, research on high-temperature-resistant Al alloys with enhanced mechanical performance has intensified further [6–9].

The high-temperature resistance of Al alloys can be further enhanced by increasing the thermal stability of the main strengthening precipitates, e.g., θ′ in the Al–Cu system [10,11], and/or by inducing the precipitation of dispersoids enriched with slow-diffusing transition metals (e.g., Zr, V, and Mo) [12–15]. However, only a limited fraction of dispersoids containing slow diffusers can be obtained in conventional casting, mainly because of the low solid solubility of these slow-diffusing transition metals in α-Al [16,17]. Therefore, increasing the thermal stability of the θ′ phase and reducing its coarsening rate could be an effective approach to improving the performance of high-temperature-resistant aluminum alloys [4,18].

Recent studies have revealed that θ′ precipitates remain stable at much higher temperatures in Al–Cu alloys than in Al–Si–Cu–Mg alloys [18]. This suggests that certain solute elements, e.g., Si, tend to accelerate the θ′-to-θ transformation, thus degrading the mechanical properties of the alloy [19]. This behavior also explains why Al–Cu-based alloys are stronger at elevated

* Corresponding author.
E-mail address: kun.liu@uqac.ca (K. Liu).

https://doi.org/10.1016/j.jallcom.2020.154305
0925-8388/

temperatures than Al–Si–Cu-based alloys [20]. However, some elements have been found to stabilize the θ′ phase at higher temperatures in the Al–Cu system [4]. Zr and Nb can reportedly enhance the precipitation of θ′ precipitates and slow the growth and coarsening of the θ′ phase [21,22]. The strengthening effect of θ′ has been found to increase with minor additions of Sn, Cd, and In Refs. [23,24].

The addition of Mg to Al–Cu alloys has been the subject of multiple studies [25–27]. Researchers recently attempted to improve the high-temperature mechanical properties of Al–Cu alloys by promoting the precipitation of the Ω phase (Al_2Cu), which is compositionally similar to, but crystallographically different from, the θ′ phase; the Ω phase is also generally considered to be more resistant to coarsening than is the θ′ phase [28]. The Ω phase was found to have good coarsening resistance and a good strengthening effect in Al–Cu alloys up to 200 °C. However, at higher temperatures, the Ω phase coarsens quickly and is eventually transformed into the equilibrium θ phase, losing its strengthening effect [25].

It is worth investigating the effect of very small amounts of Mg on the thermal stability of the θ′ phase because the Ω phase is unlikely to precipitate in Al–Cu alloys at lower Mg levels [29]. Previous studies have found that adding Mg can affect the precipitation of the θ′ phase [26,30]. However, the thermal stability and coarsening kinetics of the θ′ phase at temperatures above 200 °C have received less attention. Therefore, further understanding of the role of Mg in the precipitation of the θ′ phase and, in particular, in its thermal stability and coarsening resistance at elevated temperature (300 °C) is essential. This study investigates the effect of microalloying with Mg on the precipitation and coarsening behavior of the θ′ phase and on the mechanical performance of high-temperature-resistant Al–Cu 224 cast alloy.

2. Experimental procedure

The chemical composition of the Al–Cu 224 cast alloys investigated in this study is shown in Table 1 (all the alloy compositions are in wt.% unless indicated otherwise). Tensile test bars were cast in a Stahl mold (ASTM B-108) at Arvida Research and Development Centre of Rio Tinto Aluminum, Quebec. The average secondary dendrite arm spacing in the central region of the as-received bars was measured to be ~20 μm for all the experimental alloys, indicating a consistent temperature profile and cast conditions during casting.

T7 heat treatment of all the experimental alloys was performed in an air-circulating furnace. Two-step solution heat treatment was applied, with the first step at 495 °C for 2 h and the second step at 528 °C for 14 h, and was followed by quenching in water at room temperature. Aging was performed at 200 °C for 4 h. To investigate the thermal stability of the experimental alloys, some of the T7 heat-treated samples were further held at 300 °C for various times (100, 500, and 1000 h).

Optical microscopy and transmission electron microscopy (TEM) with energy-dispersive spectroscopy (EDS) were used to investigate the microstructure. Samples for metallographic observations were prepared by the standard technique. To reveal grain boundaries, the polished samples were immersed in 0.5% HF etchant for ~15 s. A TEM thin foil was prepared using twin-jet electrochemical equipment at a voltage of 15 V in a solution consisting of 67% methanol and 33% nitric acid at a temperature ranging between −20 and −30 °C. TEM observations of precipitates in the α-Al matrix were made near the [001] axis zone under the g200 beam condition. The volume fraction and number density of the θ″ and θ′ particles were quantitatively analyzed using the methods described in Refs. [31,32]. The TEM foil thickness was measured using the two-beam convergent-beam diffraction pattern method. Differential scanning calorimetry (DSC, PerkinElmer DSC 8000) analyses were performed on the samples at a heating rate of 10 °C/min. Three samples per condition were tested to ensure that the DSC curves were representative.

The tensile properties of all the experimental alloys were tested using an Instron universal testing machine at a strain rate of 10^{-3} s^{-1}. The compressive yield strength (YS) of selected alloys was measured using a Gleeble 3800 thermomechanical simulator unit at a strain rate of 10^{-3} s^{-1} and a total strain of 0.2. The Gleeble samples were 10 mm in diameter and 15 mm in height. At least three samples were tested for each condition. Vickers microhardness tests were conducted using a load of 100 g and a dwell time of 20 s. At least 10 hardness tests per condition were performed to determine the reproducibility of the results.

Table 1
Chemical composition of the experimental alloys (wt. %).

Alloys	Cu	Mg	Si	Mn	Fe	Ti	V	Zr	Al
0 Mg	4.71	–	0.09	0.33	0.15	0.20	0.17	0.14	bal.
0.09 Mg	4.74	**0.09**	0.08	0.33	0.14	0.22	0.17	0.13	bal.
0.13 Mg	4.74	**0.13**	0.09	0.33	0.15	0.21	0.17	0.13	bal.
0.19 Mg	4.74	**0.19**	0.10	0.33	0.15	0.20	0.17	0.14	bal.
0.23 Mg	4.74	**0.23**	0.10	0.32	0.15	0.20	0.18	0.14	bal.

3. Results and discussion

3.1. As-cast and solutionized microstructures

Fig. 1 shows typical representative microstructures of the as-cast and solutionized 0.19 Mg alloy. The average grain size of all the investigated alloys was found to be ~170 μm, indicating that Mg addition had no apparent effect on the grain structure and size of the alloys. The as-cast microstructure (Fig. 1b) comprises the α-Al matrix, plate-like $Al_3(ZrVTi)$ particles, and the Al_7Cu_2Fe, Al_2Cu, and Mg_2Si eutectic phases. No apparent difference among the microstructures of the as-cast experimental alloys was observed, except that the Mg_2Si particles formed only at a higher Mg content (0.19%). In the microstructure after solution treatment (Fig. 1c), the Mg_2Si and most of the Al_2Cu were dissolved in the aluminum matrix, whereas dissolution of $Al_3(ZrVTi)$ and Al_7Cu_2Fe remained unfavorable. The solutionized samples were observed using TEM to determine whether solid-state precipitation of Zr- or V-rich dispersoids can occur during solution treatment; no evidence was found for the presence of any type of dispersoids in the aluminum matrix.

3.2. Mechanical properties and microstructure at ambient temperature

The ambient-temperature mechanical properties of the experimental alloys under T7 conditions are shown in Fig. 2. Microalloying with Mg significantly increased the tensile strength. The YS at a 0.2% offset strain and the ultimate tensile strength (UTS) increased from 189 to 349 MPa in the 0 Mg alloy to 393 and 466 MPa in the 0.13 Mg alloy, respectively. At higher Mg contents (0.19% and 0.23%), the UTS decreased moderately, whereas the YS remained almost unchanged, suggesting that further increasing the Mg level does not increase the strengthening contribution. With increasing Mg content, the elongation of the alloys decreased steadily from 15% at 0% Mg to just 2.4% at 0.23% Mg. The tensile test results indicate that microalloying with 0.1%–0.15% Mg is sufficient to significantly improve the tensile properties.

To reveal the microstructural changes resulting from Mg addition, detailed TEM investigations were performed on three typical

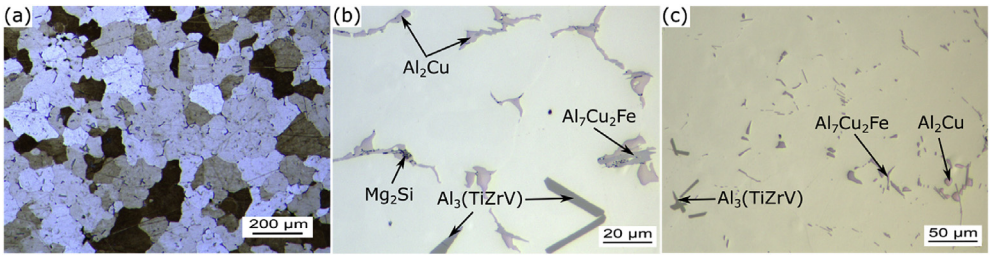

Fig. 1. Typical optical micrographs showing (a) grain structure and (b,c) intermetallic phases of alloy with 0.19% Mg under the as-cast (a,b) and solutionized (c) conditions.

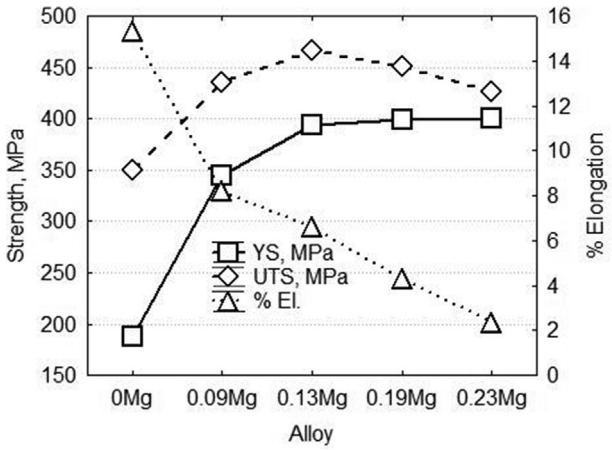

Fig. 2. Tensile properties of experimental alloys at ambient temperature under T7 conditions.

alloys, namely, the 0 Mg, 0.13 Mg, and 0.19 Mg alloys. Fig. 3a shows a bright-field TEM image of the 0 Mg alloy under T7. This condition is characterized by the presence of mainly θ″ precipitates; this finding is consistent with the corresponding selected area diffraction pattern (SADP, Fig. 3b), which shows discontinuous streaks along (200)α with maxima at the ¼, ½, and ¾ positions. The spot reflections in the SADP at the (011)α positions represent θ″ precipitates, the broad faces of which are perpendicular to the beam [25]. In addition to the predominant θ″ precipitates, θ′ precipitates with staircase-shaped structure were occasionally observed, indicating nucleation on dislocations (Fig. 3c) [33].

The typical precipitation microstructure of the 0.13 Mg alloy after T7 treatment is shown in Fig. 4a. This alloy is characterized by the presence of mainly θ′ precipitates. The spots and strikes, indicated by arrows in the corresponding SADP (Fig. 4b), are characteristic features of the θ′ phase [34]. A few θ″ precipitates consisting of several multilayers were also occasionally observed as a minor phase (Fig. 4c); however, the SADP reveals no information about this phase owing to its low volume fraction.

Fig. 5 shows TEM micrographs representing the 0.19 Mg alloy under T7 conditions. Like that of the 0.13 Mg alloy, the microstructure of this alloy is largely dominated by θ′ precipitates lying parallel to the (001)α planes, and diffraction spots representing this phase appear in the SADP (Fig. 5b). A comparison of the two Mg-containing alloys shows no apparent difference in the average length, thickness, and number density of the θ′ precipitates.

The TEM results for the T7 heat-treated experimental alloys (Figs. 3, Fig. 4, and Fig. 5) clearly show that minor addition of Mg to the experimental alloy promoted the precipitation of fine and homogeneously distributed θ′ particles. According to the literature, the θ′ phase can be precipitated in one of two ways: by either (1) independent nucleation and growth involving the dissolution of θ″ [34,35] or (2) direct nucleation and growth by rearrangement of atoms in the θ″ phase [19,34]. Direct nucleation of the θ′ phase within the θ″ phase has been found to be favored when the alloy contains certain elements such as Sn [19], Cd [23,36], In Refs. [23,36], and Au [37]. High-resolution characterization of the Mg-containing alloy showed that only the upper part of the precipitate exhibited θ″ phase structure, whereas the lower part is believed to be the θ′ phase (Fig. 4c). This result suggests that the θ′ phase nucleated directly within the θ″ phase by atomic-scale rearrangement of elements, rather than by independent nucleation of the θ′ phase at the expense of the θ″ phase [19,34].

DSC analyses of the 0 Mg and 0.13 Mg alloys were performed to reveal the effect of Mg on the kinetics of the θ″-to-θ′ transformation. The first peak in the DSC curves of the T7 samples is associated with dissolution of the θ″ particles (Fig. 6a); however, the area under the peak is much larger for the 0 Mg alloy than for the 0.13 Mg alloy, suggesting that the fraction of θ″ particles in the former was much higher than that in the latter, in agreement with the microstructural observations (Figs. 3 and 4). The θ′ precipitation

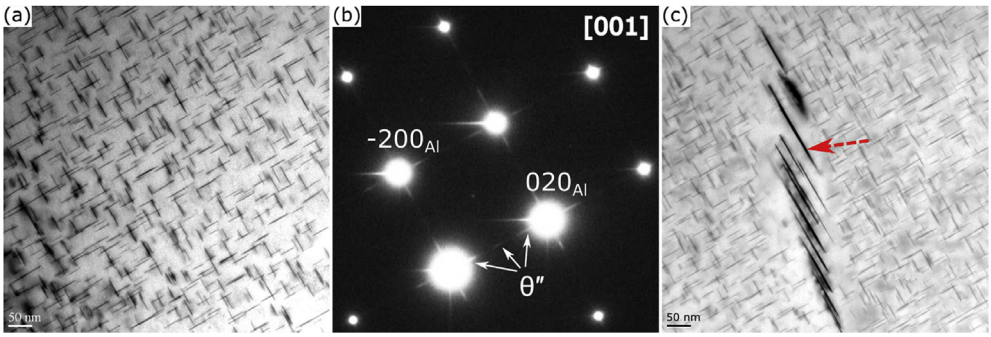

Fig. 3. Bright-field TEM images (a,c) and corresponding SADPs (b) of the 0 Mg alloy viewed along <001>$_{\alpha\text{-Al}}$. The arrow in (c) indicates θ′ precipitates that nucleated on a dislocation, forming a staircase structure.

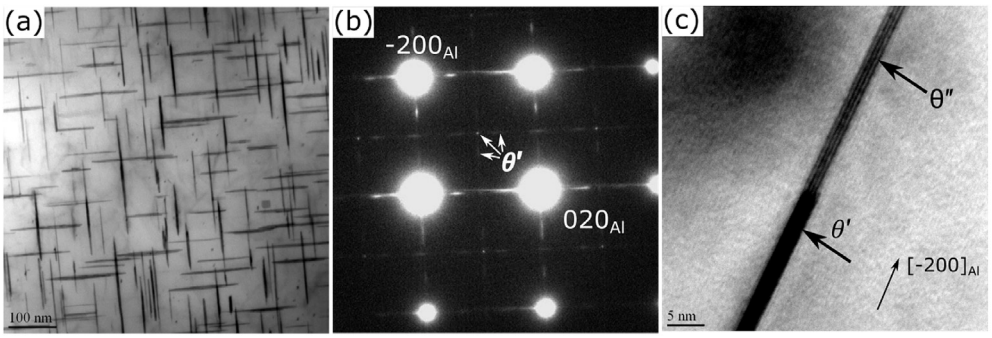

Fig. 4. Bright-field TEM images (a,c) and corresponding SADPs (b) of the 0.13 Mg alloy viewed along <001>$_{\alpha\text{-Al}}$.

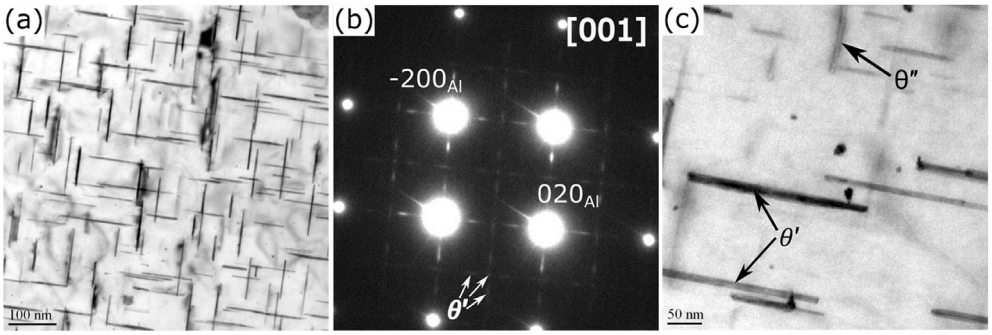

Fig. 5. Bright-field TEM images (a,c) and corresponding SADP (b) of the 0.19 alloy viewed along <001>$_{\alpha\text{-Al}}$.

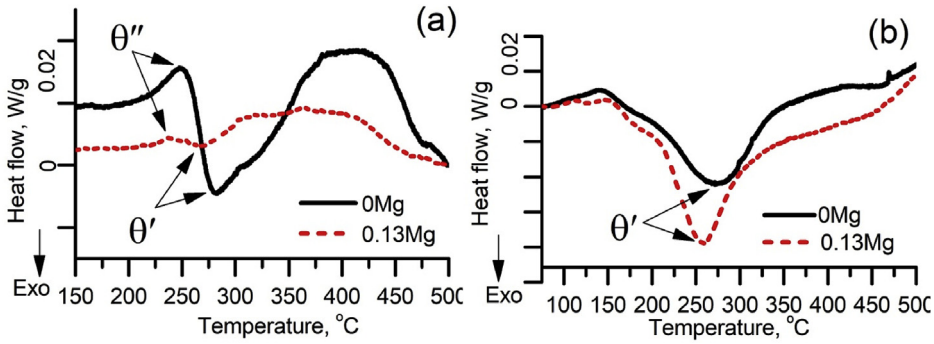

Fig. 6. Typical DSC curves during heating of 0 Mg and 0.13 Mg alloys: (a) T7-treated and (b) solutionized and quenched samples.

reaction (second peak) shows a similar tendency; i.e., the magnitude of the θ′ precipitation reaction is much smaller in the 0.13 Mg alloy than in the 0 Mg alloy, as most of the θ′ phase appeared during aging in the former (Fig. 4). The DSC curves of the solutionized samples (Fig. 6b) also confirm the role of Mg in accelerating the precipitation of the θ′ phase, as the peak temperature of θ′ precipitation, at which the precipitation rate is highest, is ~20 °C lower in the 0.13 Mg alloy. Moreover, the precipitation temperature range of the Mg-containing alloy is much narrower than that of the alloy without Mg, which could be a result of the enhancement of the nucleation rate upon Mg addition.

It is well known that in precipitation-hardened Al–Cu alloys, the mechanical strength at ambient temperature is controlled mainly by the precipitate characteristics, such as the type, size, and volume fraction of precipitates formed during aging. The observed difference in the mechanical strengths of the experimental alloys (Fig. 2) can be better explained by adopting a strength model [31].

Owing to their coherence with the α-Al matrix and shearability, the θ″ precipitates contribute to the strengthening by various factors, such as order strengthening, interfacial strengthening, coherency strengthening, and modulus mismatch strengthening, all of which result from interactions between dislocations and precipitates [22,38]. The strengthening effects of modulus mismatch and order strengthening are reportedly negligible [22,39]. The contribution of the θ″ precipitates to the critically resolved shear stress (CRSS), $\Delta\tau$, due to coherency strengthening can be estimated as [39].

$$\Delta\tau = 4.1 \cdot G \cdot \left|\varepsilon^{3/2}\right| \cdot \left[\frac{f d_t}{2b}\right]^{1/2} \quad (1)$$

where G is the shear modulus of the α-Al matrix (28 GPa [22]), ε is the lattice strain (0.006 [22]), f is the volume fraction of precipitates, b is the magnitude of the Burgers vector for aluminum

(0.284 nm [40]), and d_t is the effective width of the θ″ precipitates. The increase in the CRSS due to interfacial strengthening of the θ″ phase results from the formation of new interfaces during its interactions with dislocations [22,38] and can be estimated as [38].

$$\Delta\tau = \left(\frac{0.908 d_t}{t_t^2}\right)\left(\frac{bf}{\Gamma}\right)^{\frac{1}{2}}\gamma_i^{\frac{3}{2}}\Delta\tau = \left(\frac{0.908 d_t}{t_t^2}\right)\left(\frac{bf}{\Gamma}\right)^{\frac{1}{2}}\gamma_i^{\frac{3}{2}} \quad (2)$$

where t_t is the effective thickness of the θ″ precipitates; γ_i is the interfacial energy (0.21 J/m^2 [31]), and Γ represents the dislocation line tension, which is expressed as

$$\Gamma = \frac{Gb^2}{2\pi} ln\sqrt{\frac{d_t^2}{2b^2 f}} \quad (3)$$

The CRSS increments due to coherency and interfacial strengthening by the θ″ precipitates in the 0 Mg alloy are calculated as 59.2 and 5 MPa, respectively. The results suggest that the interfacial strengthening effect of the θ″ precipitates with the observed characteristics in the 0 Mg alloy (Table 2) is negligible compared to their contribution to coherency strengthening. The YS increment due to precipitates, σ_p, is obtained as [22].

$$\sigma_p = M \cdot \Delta\tau \quad (4)$$

where M is the Taylor factor ($M = 3$ [22]). As shown in Table 2, the σ_p value of the 0 Mg alloy is estimated to be ~180 MPa, which accounts for ~80% of the experimentally measured YS. This suggests reasonable agreement between the estimated YS increment due to θ″ precipitates and the measured YS, because the strengthening effects of the other mechanisms, such as solid solution hardening and grain size hardening in the T7-treated alloys, remain relatively low.

Further, the θ′ particles that formed in the Mg-containing alloys are non-shearable; therefore, they contribute to alloy strengthening by the Orowan looping mechanism [22]. The CRSS increment due to θ′ particles with the observed characteristics (Table 2) was estimated as [31].

$$\Delta\tau = \left(\frac{Gb}{2\pi\sqrt{1-\nu}}\right)\left(\frac{1}{1.23\frac{1.03}{\sqrt{N_v d_t}} - \frac{\pi d_t}{8} - 1.061 t_t}\right) \times \left(ln\frac{0.981\sqrt{d_t t_t}}{b}\right) \quad (5)$$

where N_v is the number density of θ′ precipitates, and ν is the Poisson ratio (0.33 for face-centered cubic metals [22]). The YS increments due to θ′ particles in the 0.13 Mg and 0.19 Mg alloys are estimated to be similar, ~300 MPa, which confirms that the θ′ precipitates observed in the Mg-containing alloys make a much larger contribution to strengthening of the alloy than the θ″ precipitates observed in the 0 Mg alloy (Table 2).

3.3. Mechanical properties and microstructure at elevated temperature

Fig. 7a shows the tensile properties of the experimental alloys at 300 °C after stabilization at 300 °C for 100 h following T7 treatment before mechanical testing. The results clearly show that the Mg-containing alloys, in particular the alloys with 0.09% and 0.13% Mg, have much higher YS values at elevated temperature than the alloy without Mg. Microalloying with Mg increased the YS from 98 MPa in the 0 Mg alloy to 120–130 MPa in the 0.09 Mg and 0.13 Mg alloys, representing a 25% improvement. As the Mg increased further, to 0.23%, the YS and UTS both tended to decrease. The ductility of the experimental alloys (%El) at elevated temperature was generally very good; it varied between 12% and 18%, and it was not greatly affected by the Mg content.

The compressive YS of three typical alloys under T7 conditions and in the stabilized state was also tested at 300 °C (Fig. 7b). The YS of both Mg-containing alloys (0.13% and 0.19%) was significantly higher than that of the base alloy. The results of compression testing of the stabilized samples (Fig. 7b) were similar to those of high-temperature tensile testing (Fig. 7a). A low Mg content (0.13%) maintained the strength more effectively than a high Mg content. The YS at 300 °C of the 0.13 Mg alloy increased by 30% relative to that of the 0 Mg alloy (142 vs. 111 MPa), whereas the YS of the 0.19 Mg alloy was 10% higher than that of the 0 Mg alloy.

Fig. 8 shows the typical precipitation microstructures of the experimental alloys after stabilization, in which all the precipitates in the three alloys are the θ′ phase, as determined from the corresponding SADP [41]. The θ′ precipitates are in a coarsening stage, as (1) the corresponding SADPs reveal clearly defined spots featuring the θ′ phase (Fig. 8d,e,f), in contrast to the streaks observed as a characteristic feature of the θ′ phase in the T7-treated alloys (Figs. 4b and 5b), and (2) the length of the θ′ particles is more broadly distributed (Fig. 8a,b,c) than that of the T7 samples, which show a narrow length distribution of the θ′ particles (Figs. 4a and 5a).

The main distinctive feature of the three experimental alloys is that the θ′ precipitates in the Mg-containing alloys are much finer and denser than those in the alloy without Mg (Fig. 8). The quantitative θ′ characteristics are listed in Table 3. The average length and thickness of the θ′ particles in the 0.13 Mg alloy are smaller, and their number density is significantly higher than those of the 0 Mg alloy. As the Mg content increases further, from 0.13% to 0.19%, the average thickness and length of the θ′ particles remain unchanged, but their number density decreases noticeably, from 406 to 226 μm^{-3}. In addition, a few coarse precipitates lying on the $\{210\}_{Al}$ planes are observed in the 0.19 Mg alloy (Fig. 8c), and these precipitates are identified as the S (Al_2CuMg) phase, as this phase has been reported to precipitate parallel to the $\{210\}_{Al}$ planes in Mg-containing Al–Cu alloys [42]. The S particles are much larger than the θ′ particles, and their coarsening is believed to occur at the expense of the θ′ particles.

The finer and denser precipitates observed in the Mg-containing alloys are more effective for alloy strengthening at elevated temperature, which explains why the YS at 300 °C of the Mg-containing alloys, in particular the alloy with 0.13% Mg, is remarkably higher

Table 2
Summary of quantitative TEM results of θ″ and θ′ phase characteristics in experimental alloys under T7 conditions.

Alloy	Quantified particles	Length, μm	Thickness, μm	Number density, μm^{-3}	Volume fraction	Δτ, MPa	σ_p, MPa
0 Mg	θ″	0.0315 (±0.009)	0.0032 (±0.001)	8958.2	0.022	59.2	177.5
0.13 Mg	θ′	0.0872 (±0.035)	0.0041 (±0.001)	1754.8	0.043	101.3	303.9
0.19 Mg	θ′	0.0822 (±0.033)	0.0040 (±0.001)	1840.3	0.040	96.5	290.0

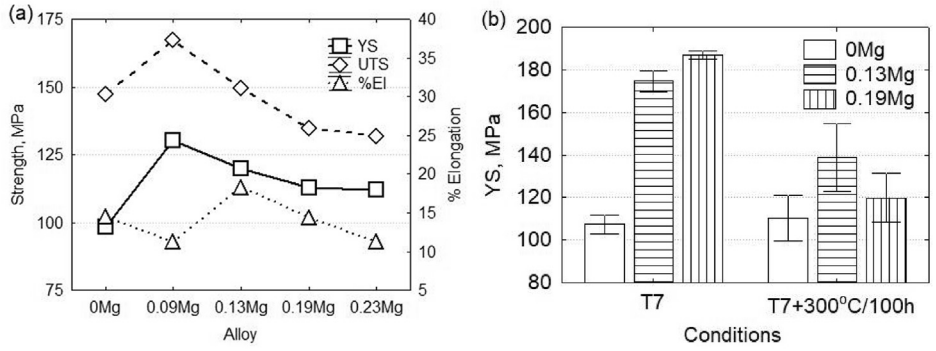

Fig. 7. (a) High-temperature tensile properties of the experimental alloys stabilized at 300 °C for 100 h following T7 treatment and (b) high-temperature compressive YS of the experimental alloys under T7 conditions and after stabilization treatment (T7 + 300 °C, 100 h).

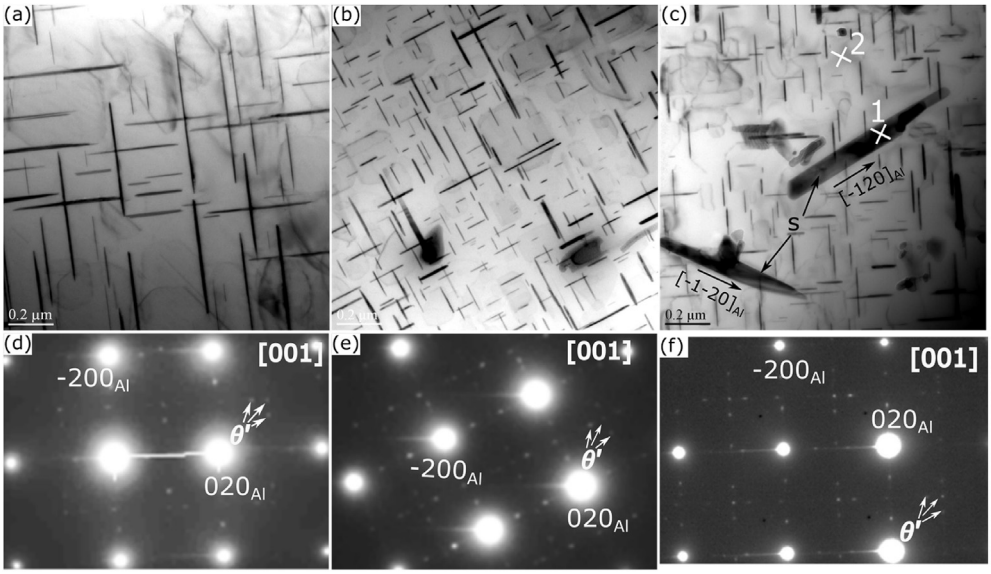

Fig. 8. Bright-field TEM images (a, b, c) and corresponding SADPs (d, e, f) viewed along <001>$_{\alpha\text{-Al}}$ of 0 Mg alloy (a and d), 0.13 Mg alloy (b and e), and 0.19 Mg alloy (c and f). Cross-marks numbered 1 and 2 in Fig. 8c indicate the regions where the TEM-EDS analyses were performed.

Table 3
Quantitative TEM results for θ′ characteristics in experimental alloys after stabilization.

Alloy	Quantified precipitates	Length, μm	Thickness, μm	Number density, μm^{-3}	Volume fracrion
0 Mg (300 °C/100 h)	θ′	0.604 (±0.36)	0.027 (±0.005)	7.0	0.054
0.13 Mg (300 °C/100 h)	θ′	0.110 (±0.06)	0.012 (±0.001)	405.9	0.048
0.19 Mg (300 °C/100 h)	θ′	0.122 (±0.01)	0.011 (±0.003)	226.0	0.030
0.13 Mg (300 °C/1000 h)	θ′	0.250 (±0.152)	0.013 (±0.004)	75.4	0.051

Table 4
TEM-EDS results for the S phase (1) and the matrix (2) shown in Fig. 8c.

Analyzed phases	EDS results (wt.%)				
	Cu	Mg	Si	Mn	Al
S—Al_2CuMg	15.28	3.77	4.10	7.56	67.21
α-Al	5.56	0.16	—	0.27	93.58

than that of the alloy without Mg (Fig. 7). The fact that the 0.19 Mg alloy has a lower YS after stabilization than the 0.13 Mg alloy can be attributed to precipitation of the coarse S phase. It had two effects: (1) the S phase consumed some Cu solutes, thus remarkably reducing the number density and volume fraction of the θ′ particles (Table 3), and (2) some Mg, Mn, and Si, which are expected to remain in solid solution, were bound to the S phase (Table 4), thus reducing the solid solution hardening contribution of the solutes somewhat.

To understand why the θ′ precipitates in the Mg-containing alloy are significantly finer than those in the alloy without Mg, the as-aged microstructures of these two alloys were examined. The θ′ precipitates that formed during aging (T7 treatment) in the Mg-containing alloy experienced only coarsening during stabilization at 300 °C. The coarsening proceeded mainly by lateral

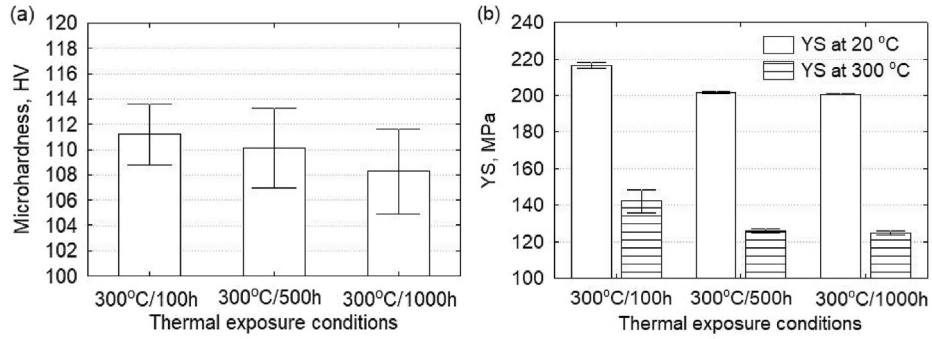

Fig. 9. Microhardness (a) and room- and high-temperature YS (b) of 0.13 Mg alloy after exposure at 300 °C for various times.

growth/lengthening of the plates, which is governed by the interfacial and strain energy anisotropies [43]. By contrast, the thickening of the precipitates was rather slow and required ledge nucleation [44]; its rate has been found to be temperature-dependent [45]. More specifically, the formation of precipitates at low temperature (T7 treatment), e.g., 200 °C, has been found to involve limited nucleation density of the thickening ledges [45]. During stabilization, further nucleation of the ledges on the pre-existing θ′ particles is limited because Cu solutes from the shrinking precipitates preferentially move toward the growing lateral surfaces. Thus, it is inferred that the limited ledge nucleation and dominant lateral growth of larger precipitates at the expense of smaller ones during preconditioning of the Mg-containing alloy resulted in the broad size distribution and higher number density of θ′ precipitates (Fig. 8b).

By contrast, the alloy without Mg under T7 conditions is composed predominantly of θ″ particles. When the alloy is treated at 300 °C during stabilization, the θ″ particles tend to first change into the θ′ phase and then become coarse. However, at elevated temperature (300 °C), the driving force for nucleation of the θ′ phase becomes lower, and the diffusion of Cu is much greater, leading to activation of a limited number of nucleation sites and fast growth of θ′ particles [35,45]. Furthermore, quick dissolution of θ″ particles at 300 °C can satisfy the solute requirement for both lateral and ledge growth [45], and thus induces the precipitation of thicker θ′ particles in the early stages of stabilization. Once a few relatively thick (coarse) precipitates are formed, their coarsening rate increases owing to the larger surface area of the advancing precipitate edges. Therefore, stabilization at elevated temperature clearly caused significant coarsening of the θ′ plates in the 0 Mg alloy (Fig. 8a and Table 3).

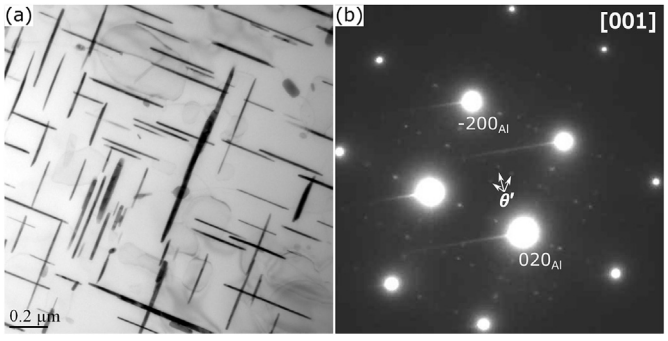

Fig. 10. (a) Bright-field TEM image and (b) the corresponding SADP of 0.13 Mg alloy viewed along <001>$_{\alpha\text{-Al}}$ after exposure at 300 °C for 1000 h.

3.4. Long-term thermal stability

The long-term thermal stability of the mechanical properties during service is an important feature of high-temperature-resistant aluminum alloys. In this study, after stabilization (T7 treatment plus treatment at 300 °C for 100 h), thermal exposure at 300 °C was continued for up to 1000 h to assess the long-term thermal stability of the material. Fig. 9 shows the evolution of the microhardness and YS of the 0.13 Mg alloy during prolonged thermal exposure. The microhardness decreased slightly from 111 HV at 100 h to 108 HV after 1000 h (Fig. 9a). The YS after stabilization (300 °C, 100 h) was 217 and 140 MPa at 20 and 300 °C, respectively (Fig. 9b). Prolonging the thermal exposure to 500 h caused a moderate drop in the YS (by ~10%) at both room and high temperatures. As the exposure time was increased further to 1000 h, no further changes in the YS were observed. Specifically, the YS of the 0.13 Mg alloy after 1000 h at 300 °C was still 202 and 125 MPa at 20 and 300 °C, respectively. Importantly, the Mg-containing alloy has not only high strength at high temperature but also an excellent balance between the ambient-temperature and high-temperature mechanical properties, so this material is expected to exhibit reliable and robust performance during long-term service.

TEM investigation of the 0.13 Mg alloy after 1000 h revealed that the precipitates were still the θ′ phase, which retained its plate-like

Table 5
Comparison of the YS at 300 °C of various cast aluminum alloys.

#	Alloys	YS at 300 °C –315 °C*		Reference
		100 h	1000 h	
1	224-(0 Mg)-T7	110	–	Present study
2	224-(0.13 Mg)-T7	**142**	**125**	Present study
3	224-T7	110 *	105 *	[47]
4	240-T7	105 *	90 *	[47]
5	242-T7	52 *	45*	[47]
6	201-T7	–	55 *	[47]
7	Al5CuMg-T6	60 **	–	[10]
8	Al5CuNiMnZr-T6	105 **	–	[10]
9	356-T6	28 *	24 *	[47]
10	356ZrV-T6	41	–	[5]
11	3560.5Cu-T7	33	–	[12]
12	3560.5Cu0.3Mo-T7	47	–	[12]
13	319-T5	52 *	48 *	[47]
14	319-T7	51	34	[48]
15	3190.25Mn0.3Mo-T7	60	54	[48]
16	Al5Si4CuZrVTi-T7	63	–	[5]

Note: * Test temperature and thermal exposure temperature is 315 °C [49]. ** Thermal exposure is at 300 °C for 200 h [11].

shape (Fig. 10); the quantitative results are shown in Table 3. A comparison of two exposure times (100 h in Figs. 8b and 1000 h in Fig. 10a) shows that the coarsening of the precipitates was dominated by lengthening, as the average length of the θ′ phase increased from 0.11 μm after 100 h to 0.25 μm after 1000 h, whereas the thickness remained unchanged. It is reasonable to think that only moderate coarsening occurred during prolonged thermal exposure, confirming the long-term thermal stability of the θ′ phase at 300 °C, which is the key point for preserving the high-temperature properties, where the YS exceeded 125 MPa at 300 °C after 1000 h. It is also interesting that the YS at 300 °C of the 0.13 Mg alloy after 1000 h (125 MPa) was even higher than that of the 0 Mg alloy after 100 h (111 MPa), because the θ′ precipitates in the 0.13 Mg alloy after 1000 h were still finer and denser than those of the 0 Mg alloy after 100 h (Table 3).

3.5. Comparison of high-temperature strength of various cast aluminum alloys

The cast aluminum alloys that are most frequently used to fabricate engine blocks and cylinder heads fall into two main groups [5]:

- Al–Si–Mg 356-type alloys containing 7–10 wt% Si and 0.25–0.45 wt% Mg and strengthened with β″/β′ Mg_2Si precursors;
- Al–Si–Cu–Mg 319-type alloys containing 5–9 wt.% Si and 3–4 wt.% Cu and strengthened with θ″/θ′ Al_2Cu precursors.

Aluminum alloys based on the 356 and 319 types have excellent ductility and strength at ambient temperature, but their elevated-temperature strengths are quite limited (#9, 13, and 14 in Table 5). The operating temperature has been increasing continuously (toward 300–350 °C) with the development of new generations of engines [46]. Recent studies have explored the introduction of thermally stable dispersoids by adding transition elements in both types of alloys (#10, 11, 12 in 356 alloys and #15, 16 in 319 alloys in Table 5), which considerably improved the YS at elevated temperature. However, owing to the relatively low volume fraction of the dispersoids, their strengthening effect remains relatively small.

By contrast, some Al–Cu alloys exhibit much better high-temperature strength and high thermal stability (#3 and 4) than the 356 or 319 alloys. The 0 Mg alloy (#1) in this work also showed a relatively high YS at 300 °C, which is consistent with the results in the literature (#3). The present work demonstrated that appropriate microalloying with Mg can further improve the high-temperature strength. As shown in Table 5, the 0.13 Mg alloy (#2) showed the highest YS (142 MPa at 300 °C) and was far superior to all the other cast aluminum alloys. Owing to the excellent stability of the θ′ precipitates, its YS after 1000 h at 300 °C was still 125 MPa, which greatly exceeded the YS of all the other alloys, making this material more suitable for long-term service at elevated temperatures.

4. Conclusions

The precipitation behavior and its effects on the ambient- and high-temperature mechanical properties and thermal stability of high-temperature-resistant Al–Cu 224 alloys microalloyed with Mg were investigated. The following conclusions can be drawn:

- In the absence of Mg, the precipitates in the Al–Cu 224 alloy under T7 conditions were predominantly the θ″ phase. Microalloying with Mg enhanced the precipitation of the θ′ phase during aging, producing fine, dense, and uniformly distributed θ′ precipitates. These precipitates were much more effective for alloy strengthening than the θ″ precipitates in the alloy without Mg, in good agreement with the results of strength modeling based on the quantitative characteristics of the precipitates.
- During stabilization at 300 °C for 100 h after T7 treatment, the precipitates of all the alloys were mostly θ′ particles that had undergone coarsening. The θ′ precipitates in the Mg-containing alloys were much finer and denser than those in the alloy without Mg; consequently, the Mg-containing alloys had remarkably improved high-temperature strength.
- The alloys with low Mg levels (0.09%–0.13%) were found to retain their strength better at elevated temperatures. The YS at 300 °C of the 0.13% Mg alloy was as high as 140 MPa. With increasing Mg content (>0.19%), coarse S (Al_2CuMg) particles appeared, reducing the number density of the θ′ particles and decreasing the high-temperature strength.
- The θ′ precipitates in the 0.13% Mg alloy remained thermally stable during long-term thermal exposure at 300 °C for up to 1000 h. The YS of the alloy after 1000 h at 300 °C was still 202 and 125 MPa at 20 and 300 °C, respectively, giving the alloy an excellent balance between the ambient-temperature and high-temperature mechanical properties for reliable and robust performance.
- The high-temperature strength and thermal stability of the Mg-containing alloys were far superior to those of most cast aluminum alloys, indicating that they are a promising lightweight material for high-temperature applications.

Declaration of competing interest

The authors declare that they have no known competing financial interests or personal relationships that could have appeared to influence the work reported in this paper.

Acknowledgements

The authors would like to acknowledge the financial support of the Natural Sciences and Engineering Research Council of Canada (NSERC) under the Grant No. CRDPJ 514651-17 and Rio Tinto Aluminum through the Research Chair in the Metallurgy of Aluminum Transformation at University of Quebec in Chicoutimi.

References

[1] R. Molina, P. Amalberto, M. Rosso, Mechanical characterization of aluminium alloys for high temperature applications Part1: Al-Si-Cu alloys, Metall. Sci. Technol. 29 (2011) 5–15.
[2] P. Huter, P. Renhart, S. Oberfrank, M. Schwab, F. Grün, B. Stauder, High- and low-cycle fatigue influence of silicon, copper, strontium and iron on hypo-eutectic Al–Si–Cu and Al–Si–Mg cast alloys used in cylinder heads, Int. J. Fatig. 82 (2016) 588–601.
[3] J. Rakhmonov, G. Timelli, F. Bonollo, The effect of transition elements on high-temperature mechanical properties of AlSi foundry AlloysA review, Adv. Eng. Mater. 18 (2016) 1096–1105.
[4] D. Shin, A. Shyam, S. Lee, Y. Yamamoto, J.A. Haynes, Solute segregation at the Al/theta '-Al2Cu interface in Al-Cu alloys, Acta Mater. 141 (2017) 327–340.
[5] M. Javidani, D. Larouche, Application of cast Al-Si alloys in internal combustion engine components, Int. Mater. Rev. 59 (2014) 132–158.
[6] S.K. Shaha, F. Czerwinski, W. Kasprzak, D.L. Chen, Tensile and compressive deformation behavior of the Al-Si-Cu-Mg cast alloy with additions of Zr, V and Ti, Mater. Des. 59 (2014) 352–358.
[7] S.K. Shaha, F. Czerwinski, W. Kasprzak, J. Friedman, D.L. Chen, Improving high-temperature tensile and low-cycle fatigue behavior of Al-Si-Cu-Mg alloys through micro-additions of Ti, V, and Zr, Metall. Mater. Trans. 46 (2015) 3063–3078.
[8] J. Rakhmonov, G. Timelli, F. Bonollo, Characterization of the solidification path and microstructure of secondary Al-7Si-3Cu-0.3Mg alloy with Zr, V and Ni additions, Mater. Char. 128 (2017) 100–108.
[9] J. Rakhmonov, G. Timelli, A. Fabrizi, F. Bonollo, Effect of V and Zr microalloying, and heat treatment on microstructure and mechanical properties of secondary

Al-7Si-3Cu-0.3Mg alloy, Int. J. Mater. Res. 109 (2018) 1099–1112.
[10] A. Shyam, S. Roy, D. Shin, J.D. Poplawsky, L.F. Allard, Y. Yamamoto, J.R. Morris, B. Mazumder, J.C. Idrobo, A. Rodriguez, T.R. Watkins, J.A. Haynes, Elevated temperature microstructural stability in cast AlCuMnZr alloys through solute segregation, Mater. Sci. Eng., A 765 (2019), 138279.
[11] Y.H. Gao, C. Yang, J.Y. Zhang, L.F. Cao, G. Liu, J. Sun, E. Ma, Stabilizing nano-precipitates in Al-Cu alloys for creep resistance at 300 degrees C, Mater. Res. Lett. 7 (2019) 18–25.
[12] A.R. Farkoosh, X. Grant Chen, M. Pekguleryuz, Dispersoid strengthening of a high temperature Al-Si-Cu-Mg alloy via Mo addition, Mater. Sci. Eng., A 620 (2014) 181–189.
[13] A.R. Farkoosh, X. Grant Chen, M. Pekguleryuz, Interaction between molybdenum and manganese to form effective dispersoids in an Al-Si-Cu-Mg alloy and their influence on creep resistance, Mater. Sci. Eng., A 627 (2015) 127–138.
[14] K. Liu, H. Ma, X.G. Chen, Enhanced elevated-temperature properties via Mo addition in Al-Mn-Mg 3004 alloy, J. Alloys Compd. 694 (2017) 354–365.
[15] K. Liu, X.G. Chen, Improvement in elevated-temperature properties of Al-13% Si piston alloys by dispersoid strengthening via Mn addition, J. Mater. Res. 33 (2018) 3430–3438.
[16] K.E. Knipling, Development of a nanoscale precipitation-strengthened creep-resistant aluminum alloy containing trialuminide precipitates, Northwestern University, Evanston, 2006, pp. 14–22. PhD thesis.
[17] K.E. Knipling, D.C. Dunand, D.N. Seidman, Criteria for developing castable, creep-resistant aluminum-based alloys - a review, Int. J. Mater. Res. 97 (2006) 246–265.
[18] P. Heugue, D. Larouche, F. Breton, R. Martinez, X.G. Chen, Evaluation of the growth kinetics of theta ' and theta-Al2Cu precipitates in a binary Al-3.5 Wt pct Cu alloy, Metall. Mater. Trans. 50A (2019) 3048–3060.
[19] T.K. Akopyan, N.A. Belov, N.V. Letyagin, Effect of trace addition of Sn on the precipitation hardening in Al-Si-Cu eutectic alloy, J. Occup. Med. 71 (2019) 1768–1775.
[20] J.G. Kaufman, E.L. Rooy, Aluminum Alloy Castings: Properties, Processes, and Applications, ASM International, Materials Park, 2004.
[21] S.K. Makineni, S. Sugathan, S. Meher, R. Banerjee, S. Bhattacharya, S. Kumar, K. Chattopadhyay, Enhancing elevated temperature strength of copper containing aluminium alloys by forming L1(2) Al3Zr precipitates and nucleating theta '' precipitates on them, Sci Rep-Uk 7 (2017).
[22] S. Mondol, S.K. Makineni, S. Kumar, K. Chattopadhyay, Enhancement of high temperature strength of 2219 alloys through small additions of Nb and Zr and a novel heat treatment, Metall. Mater. Trans. 49A (2018) 3047–3057.
[23] F. Lotter, D. Petschke, T.E.M. Staab, U. Rohrmann, T. Schubert, G. Sextl, B. Kieback, The influence of trace elements (in, Sn) on the hardening process of Al-Cu alloys, Phys. Status Solidi (2018) 215.
[24] C. Wolverton, Solute-vacancy binding in aluminum, Acta Mater. 55 (2007) 5867–5872.
[25] I. Zuiko, R. Kaibyshev, Aging behavior of an Al-Cu-Mg alloy, J. Alloys Compd. 759 (2018) 108–119.
[26] R. Ivanov, A. Deschamps, F. De Geuser, Clustering kinetics during natural ageing of Al-Cu based alloys with (Mg, Li) additions, Acta Mater. 157 (2018) 186–195.
[27] R. Ivanov, A. Deschamps, F. De Geuser, High throughput evaluation of the effect of Mg concentration on natural ageing of Al-Cu-Li-(Mg) alloys, Scripta Mater. 150 (2018) 156–159.
[28] S.P. Ringer, K. Hono, I.J. Polmear, T. Sakurai, Nucleation of precipitates in aged Al-Cu-Mg-(Ag) alloys with high Cu:Mg ratios, Acta Mater. 44 (1996) 1883–1898.
[29] S. Abis, P. Mengucci, G. Riontino, Influence of Si additions on the aging process of an Al-Cu-Mg-Ag alloy, Philos. Mag. A 70 (1994) 851–868.
[30] M. Song, D. Xiao, Effects of Mg and Ag elements on the aging precipitation of binary Al-Cu alloy, Sci. China E 49 (2006) 582–589.
[31] S. Roy, L.F. Allard, A. Rodriguez, W.D. Porter, A. Shyam, Comparative evaluation of cast aluminum alloys for automotive cylinder heads: Part II-mechanical and thermal properties, Metall. Mater. Trans. 48A (2017) 2543–2562.
[32] J.F. Nie, B.C. Muddle, Strengthening of an Al-Cu-Sn alloy by deformation-resistant precipitate plates, Acta Mater. 56 (2008) 3490–3501.
[33] A. Rodriguez-Veiga, B. Bellon, I. Papadimitriou, G. Esteban-Manzanares, I. Sabirov, J. LLorca, A multidisciplinary approach to study precipitation kinetics and hardening in an Al-4Cu (wt. %) alloy, J. Alloys Compd. 757 (2018) 504–519.
[34] Z. Shen, Q. Ding, C. Liu, J. Wang, H. Tian, J. Li, Z. Zhang, Atomic-scale mechanism of the $\theta'' \rightarrow \theta'$ phase transformation in Al-Cu alloys, J. Mater. Sci. Technol. 33 (2017) 1159–1164.
[35] Di David A. Porter, Kenneth E. Easterling, M. Sherif, Phase Transformations in Metals and Alloys, Taylor & Francis, London, 2008.
[36] F. Lotter, U. Muehle, M. Elsayed, A.M. Ibrahim, T. Schubert, R. Krause-Rehberg, B. Kieback, T.E.M. Staab, Precipitation behavior in high-purity aluminium alloys with trace elements – the role of quenched-in vacancies, Phys. Status Solidi 215 (2018), 1800375.
[37] Y.Q. Chen, Z.Z. Zhang, Z. Chen, A. Tsalanidis, M. Weyland, S. Findlay, L.J. Allen, J.H. Li, N.V. Medhekar, L. Bourgeois, The enhanced theta-prime (theta ') precipitation in an Al-Cu alloy with trace Au additions, Acta Mater. 125 (2017) 340–350.
[38] J.F. Nie, B.C. Muddle, Microstructural design of high-strength aluminum alloys, J. Phase Equil. 19 (1998) 543–551.
[39] L.M. Brown, R.K. Ham, in: A. Kelly, R.B. Nicholson (Eds.), Strengthening Methods in Crystals, Wiley, New York, 1971.
[40] O. Engler, C.D. Marioara, Y. Aruga, M. Kozuka, O.R. Myhr, Effect of natural ageing or pre-ageing on the evolution of precipitate structure and strength during age hardening of Al–Mg–Si alloy AA 6016, Mater. Sci. Eng., A 759 (2019) 520–529.
[41] M. Gazizov, R. Kaibyshev, Precipitation structure and strengthening mechanisms in an Al-Cu-Mg-Ag alloy, Mater. Sci. Eng., A 702 (2017) 29–40.
[42] M. Mihara, C.D. Marioara, S.J. Andersen, R. Holmestad, E. Kobayashi, T. Sato, Precipitation in an Al-Mg-Cu alloy and the effect of a low amount of Ag, Mater. Sci. Eng., A 658 (2016) 91–98.
[43] V. Vaithyanathan, C. Wolverton, L.Q. Chen, Multiscale modeling of theta ' precipitation in Al-Cu binary alloys, Acta Mater. 52 (2004) 2973–2987.
[44] L. Bourgeois, C. Dwyer, M. Weyland, J.F. Nie, B.C. Muddle, The magic thicknesses of theta ' precipitates in Sn-microalloyed Al-Cu, Acta Mater. 60 (2012) 633–644.
[45] S. Bai, X.W. Zhou, Z.Y. Liu, P. Xia, M. Liu, S.M. Zeng, Effects of Ag variations on the microstructures and mechanical properties of Al-Cu-Mg alloys at elevated temperatures, Mater. Sci. Eng., A 611 (2014) 69–76.
[46] A.R. Farkoosh, M. Pekguleryuz, Enhanced mechanical properties of an Al-Si-Cu-Mg alloy at 300 degrees C: effects of Mg and the Q-precipitate phase, Mater. Sci. Eng., A 621 (2015) 277–286.
[47] J.G. Kaufman, Properties of Aluminum Alloys: Tensile, Creep, and Fatigue Data at High and Low Temperatures, ASM International, Materials park, 1999.
[48] L. Jin, K. Liu, X.G. Chen, Evolution of dispersoids and their effects on elevated-temperature strength and creep resistance in Al-Si-Cu 319 cast alloys with Mn and Mo additions, Mater. Sci. Eng., A 770 (2020), 138554.